Low temperature conductivity of carbon nanotube aggregates

2011 J. Phys.: Condens. Matter 23 475302

(http://iopscience.iop.org/0953-8984/23/47/475302)

IOP PUBLISHING JOURNAL OF PHYSICS: CONDENSED MATTER
J. Phys.: Condens. Matter **23** (2011) 475302 (7pp) doi:10.1088/0953-8984/23/47/475302

Low temperature conductivity of carbon nanotube aggregates

M Salvato[1], M Lucci[1], I Ottaviani[1], M Cirillo[1], S Orlanducci[2], E Tamburri[2], V Guglielmotti[2], F Toschi[2], M L Terranova[2] and M Pasquali[3]

[1] Dipartimento di Fisica and MINAS Laboratory, Università di Roma 'Tor Vergata', I-00133 Roma, Italy
[2] Dipartimento di Scienze e Tecnologie Chimiche and MINAS Laboratory, Università di Roma 'Tor Vergata', I-00133 Roma, Italy
[3] Chemical and Biomolecular Engineering Department, MS-362, Rice University, Houston, TX 77251-1892, USA

Received 5 August 2011, in final form 30 September 2011
Published 10 November 2011
Online at stacks.iop.org/JPhysCM/23/475302

Abstract
We compare, over wide temperature ranges, the transport properties of single-wall carbon nanotubes arranged in the form of aligned arrays or in the form of fibres. The experimental data show that both the forms of aggregates present a crossover in the transport mechanism from three-dimensional hopping of the electrons between localized states at high temperature to fluctuation-induced tunnelling across potential barriers at low temperature. The role of the junctions formed between the bundles in the array and between the nanotubes inside the fibres is discussed on the basis of the experimental results.

(Some figures may appear in colour only in the online journal)

1. Introduction

Transport properties of aggregates of single-wall carbon nanotubes (SWCNT) have been widely studied showing interesting effects which have been explained on the basis of current theories in disordered materials [1]. All experimental data and theoretical models developed for this kind of samples emphasize the fundamental role played by interfaces effects between SWCNTs. These effects have been shown between two SWCNTs [2] or between two bundles of SWCNTs [3] or in samples formed by aggregates of SWCNTs [4]. The junctions at the interfaces are usually assumed to be generated by the action of van der Waals forces generating potential barriers for charge carriers whose characteristics (width and height) depend on the nature of the interface and on the electrical properties of the SWCNTs [1, 2]. Whatever the morphology and the nature of the SWCNT aggregate, the existence of a junction at the interface between two of them influences the charge carrier motion and, as a consequence, most of their transport properties [4]. In fact, since SWCNT aggregates are formed by randomly distributed semiconducting and metallic entities, the junctions play the role of insulating barriers along a conducting path, meaning that interesting effects such as Schottky, thermal activation, tunnel and hopping can be shown in an experiment where charge transport is monitored. To what extent these effects rule the physics of these systems could be investigated by transport measurements in a wide temperature range.

In the present paper we study the transport properties of two kinds of SWCNT aggregates: oriented arrays of SWCNT bundles and aligned SWCNT fibres. The experimental results show that, despite the difference in the barriers at the interfaces formed after the fabrication process, the transport mechanism can be interpreted by the same theoretical models, especially at low temperature where the effect of the barriers is relevant. The remainder of this paper is structured as follows: in section 2 we survey the fabrication procedure of our samples and describe the basic measurement apparatus; in section 3 we show the results for the behaviour of the resistances of the aggregates as a function of the temperature; in section 4 we present the magnetoresistance measurements; and in section 5 the measurements of the current–voltage characteristics. In sections 4 and 5 we derive important parameters that are necessary ingredients for the model presented in section 3. In section 6 we draw the conclusions.

2. Sample fabrication and measurement techniques

Aligned arrays of bundles were obtained using SWCNTs provided by CHEAP TUBES INC. (www.cheaptubesinc.com) (purity $>$ 90 wt%, ash $<$1.5 wt%) and were further purified

before deposition on the substrates. The dispersion of the CNT diameters inside the bundles is Gaussian centred at 1.5 nm with 99% of the tube diameters in the range 1–2 nm.

The SWCNT bundles have been oriented by a dielectrophoresis technique [5]. The morphology of all the produced samples was analysed by scanning electron microscope (SEM) before the transport measurements in order to check for the alignment between the electrodes and for the formation of the single junction between two of them. The presence of relevant percentages of transverse bundles causing shorts in the array was easily detected and the corresponding sample discarded. We fabricated several dozens of samples but selected for the measurements only ten chips.

Figure 1(a) shows SEM images of a representative array of SWCNT samples. The measured diameter of each bundle is about 100 nm whereas the length is about 2–3 μm, implying that about two bundles are sufficient to give a contact between the voltage electrodes, as shown in the inset of figure 1(a). These data, as well as the transport measurements shown below, can be considered representative of the samples examined.

Macroscopic SWCNT fibres are produced following the main lines of an already established methodology [6] starting from purified HiPco SWCNT powders [7, 8] containing less than 1 wt% residual metal catalyst. The fibre preparation is carried out in an anhydrous glove box (dew point −50 °C), adding 108% sulfuric acid to obtain 8 wt% SWCNT concentration. The SWCNT dope is extruded at 1.5 m min^{-1} in a static water coagulation bath using a syringe. Poly vinyl alcohol (3000 Mw) is also dissolved up to 1 wt% in the coagulation bath to slow down coagulation and improve fibre tensile strength. The fibre is then collected on wheels and dried at 110 °C. For the present experiments fibres of about 100 μm diameter and about 3 m long were produced. The fibres at the end consist of strongly aligned SWCNT having an average diameter of 1 nm and an average length of 500 nm [7]. Figure 1(b) shows an SEM image of one of the fibres under investigation while in the inset of figure 1(b) the SWCNTs emerging from the inside are shown as a sort of white tissue naps. Tens of samples were cut from the 3 m long fibres and used as samples for our experiments. As in the case of the arrays of bundles, the transport measurements shown here can be considered as very representative of all the measured samples.

Si/SiO_2 wafers, on which gold contacts for standard four-lead electrical measurements are patterned, are used as substrates for both types of investigated structures (arrays and fibres). In the case of SWCNT bundles, the distance between the inner voltage leads is $l_V = 5$ μm while the outer current leads are $l_I = 15$ μm far apart. In the case of the fibres, a longer distance is adopted: $l_V = 2$ mm for the inner voltage leads and $l_I = 6$ mm for the current electrodes. Both the structures have been oriented perpendicular to the contact probes but, while the arrays of bundles were oriented between the electrodes according to the above-mentioned dielectrophoretic technique [6], the much more rigid fibres have been manually aligned and secured to the contact pads by silver glue.

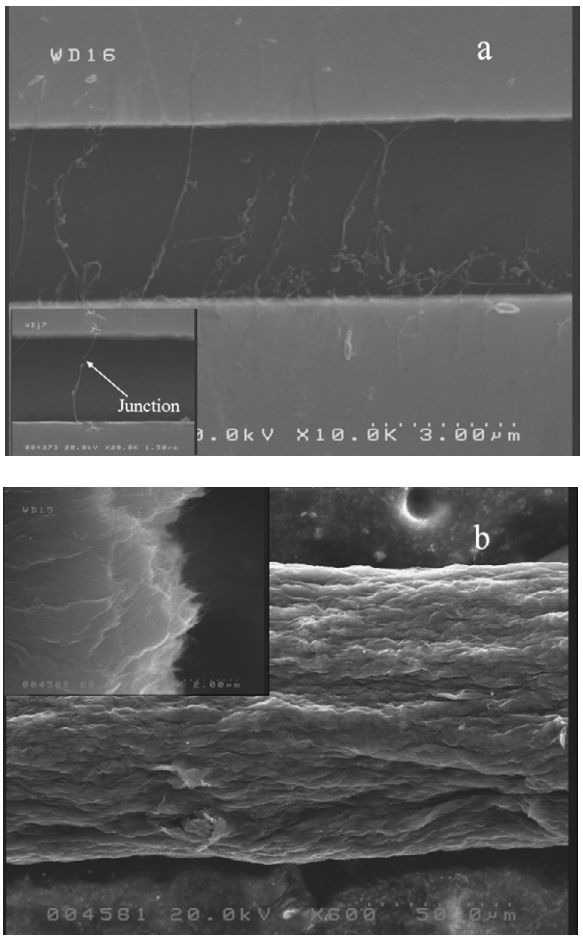

Figure 1. (a) SEM image of an array of SWCNT bundles aligned by dielectrophoresis between two voltage electrodes; inset: junction between a couple of bundles contacting the voltage electrodes. The probability of having such junctions between two bundles was higher for lower densities of the deposited tubes. (b) SEM image of a fibre manually aligned between two voltage electrodes (not shown); inset: bundles of SWCNTs coming from a section of a fibre.

All the transport measurements have been performed in a liquid ^{4}He cryostat where a pumping system allowed us to reach temperatures as low as 1 K. Magnetotransport measurements were performed in a separate liquid ^{4}He cryostat equipped with a 6 T superconducting magnet.

3. Resistance versus temperature: results and fittings

Preliminary four-lead resistance measurements for the fibres and the bundles at room temperature allowed us to estimate their resistivity. For the representative samples chosen for the present experiment, the resistivity resulted to be 5 mΩ cm and 0.4 mΩ cm in the case of the fibres and the arrays, respectively. Similar samples show values of the resistivity in a range ±2.5% around the above values for both systems.

In figure 2(a) the normalized resistance as a function of the temperature of the two representative samples (a fibre and an array) is shown. The conductance as a function of the bias

current for the same samples is reported in the inset where we see that the conductance of the SWCNTs depends on the external driving field, as expected [9, 10]. We can also see that an ohmic–non-ohmic transition is present in both the samples but at different currents. It is worth noting that Joule heating effects can be ruled out for these measurements as the cause of the ohmic–non-ohmic transition as demonstrated for other samples with similar characteristics [11]. In order to avoid any effect due to current, we analyse our samples in the ohmic region. For this reason, the samples are biased with different currents i.e. 100 nA and 1 μA for the array and the fibre, respectively. The resistance curves reported in the main panel of the figure show a different shape at low temperature: here the arrays show a finite resistance in the limit of zero temperature while the fibre tends to zero conductivity (infinite resistance) in the same limit.

Infinite resistance is expected in disordered conductors where a hopping mechanism prevails and it is well described by variable-range hopping (VRH) theory [12, 13] which gives

$$R = R_0 e^{(T_M/T)^{1/(1+d)}} \quad (1)$$

for the R versus T dependence. In this expression, d is the system dimensionality and T_M is a parameter related to the density of states at the Fermi level $N(\varepsilon_F)$ and to the localization length ξ. In three dimensions (3D), $d = 3$ and $T_M = 18.2/k_B N(\varepsilon_F)\xi^3$. In VRH theory the electronic states are localized in proximity to the impurities and the electron wavefunction appears to be confined on a distance ξ (the localization length) which is of the same order as the mean free path. Conduction takes place by hopping between two localized states separated by a distance $r = 0.38\,(T_M/T)^{1/4}\,\xi$ for $d = 3$.

A finite resistance at zero temperature, on the other hand, suggests that electrons are not completely localized but they move across the impurities even at very low temperatures where thermal activation effects can be neglected. This phenomenon is predicted by a tunnel mechanism or by fluctuation-induced tunnelling (FIT) [14] where the tunnelling of electrons across a potential barrier is supported by temperature fluctuations. This model gives

$$R = R_0 e^{T_1/(T+T_0)} \quad (2)$$

where $T_1/T_0 = \pi w\,(2m^* V_0)^{1/2}/2\hbar$, with w and V_0 the width and the height of the potential barrier, respectively, $m^* = 7.8\times 10^{-32}$ kg is the effective electron mass and $\hbar$ is the Planck constant divided by 2π. An estimate of V_0 can be obtained by the value of the experimental normalized resistance in the limit of zero temperature. In the FIT model the parameter w is an arbitrary length (directly related to the T_1/T_0 expression) which is interpreted as the van der Waals chemical bond between two SWCNTs and results to be 1.34 Å [2]. This interpretation of w is questionable both in the case of junctions between two SWCNTs and in the case of bundles because of the possible presence of distortions of the SWCNT lattice structures and the possible presence of inclusions between their interfaces. These effects, when present, would give a much larger width of the barrier. For this reason, a more straightforward procedure for the determination of w and V_0 consists in performing independent measurements such as, for example, current–voltage or magnetoresistance and relate them to the T_1/T_0 value found by R versus T. An example shall be provided in section 5.

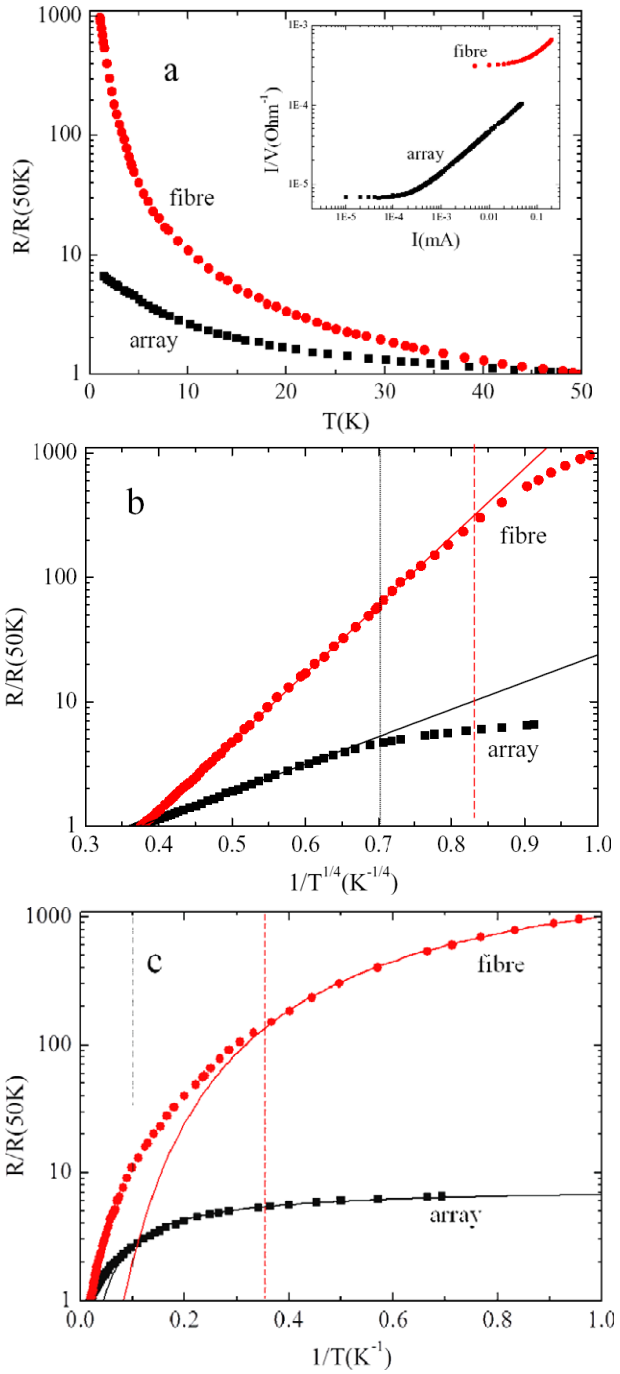

Figure 2. (a) Normalized resistance with respect to the value at $T = 50$ K of the fibre (circles) and the array (squares); inset: conductance versus bias current for both the samples. (b) Same as (a) but plotted as a function of $1/T^{1/4}$. The lines are fitted to the data following equation (1). (c) Same as (a) but plotted as a function of $1/T$. The lines are fitted to the data below T^* following equation (2). In (b) and (c) the dashed and dotted lines are drawn in correspondence to the T^* value for the fibre and the array, respectively.

Table 1. Experimental and fitting parameters for fibres and arrays.

Sample	T_M (K)	T^* (K)	T_1/T_0	a	b	V_0 (mV)	ξ (nm)	r (nm)	w (nm)
Fibre	25 600	2.0	8.02	−0.011 94	0.0019	180	4.6	15	7.6
Array	650	3.9	2.03	−0.007 8	0.000 98	520	7.7	10	1.1

We tried to interpret our $R(T)$ data on the basis of VRH and FIT theories in order to understand what transport mechanism is effective in the investigated structures. Aggregates of SWCNTs have already been studied [4, 15] but, due to the limited temperature range investigated, the conclusion in most of the cases was that just one of the two models was applicable, which generated competition between the two models for a long time. We shall see now that our experimental results demonstrate that the two models are not competing in the sense that they can both explain the experimental data, but in different temperature ranges. The crossover temperature between them, on the other hand, depends on the kind of sample analysed and, in turn, on the kind of barrier formed at the junction between SWCNTs.

In figure 2(b) the normalized resistances as a function of $1/T^{1/4}$ ($d = 3$) are reported in semilogarithmic plots for all the examined structures. All the curves are linearly approximated up to a value corresponding to a given temperature T^* (meaning that below this temperature the linear approximation fails). The values corresponding to T^* (2 K for the fibre and 3.9 K for the arrays) are indicated by the vertical lines (dashed for fibre and dotted for array) crossing the horizontal axis. Every other reciprocal temperature dependence ($d = 1$ or 2 in equation (1)) does not show the same linearity as that reported in figure 2(b), indicating that, at least in the high temperature regime, all the samples can be represented by 3D VRH equation (1) and that other dimensions as well as Coulomb-gap-based models [13] can be ruled out. The values of the T_M parameters obtained by the fit of the data are reported in table 1. Below the temperature T^* the experimental data deviate significantly from the 3D VRH prediction and a saturation of the resistance in the low temperature limit is shown. This suggests that, below T^*, a tunnel mechanism takes over in the conduction process. Figure 2(c) shows the same normalized resistance data but plotted as a function of $1/T$. The saturation in the resistance is evident, being much more marked in the case of the bundles with respect to the fibre. Nevertheless, both the array and fibres data are well fitted by the FIT model equation (2) below T^* and the obtained values of T_1/T_0, as extracted by equation (2), are reported in table 1. As in figure 2(b) the vertical lines (dashed for fibre and dotted for array) represent a visual aid for the position of the values corresponding to T^*.

4. Magnetoresistance measurements

In order to establish the degree of anisotropy in the transport properties [16] of the samples we have performed magnetoresistance measurements $\mathrm{MR} = (R(B) - R(0))/R(0)$ at 4.2 K in an external magnetic field. By orienting the field in the direction parallel or perpendicular to the bundles and fibre axes we have recorded the different response (and the degree of anisotropy). The results are shown in figure 3 where $R(0)$ and $R(B)$ are the electrical resistance measured in zero field and at a given field B, respectively. We can see that in the case of the fibre there is a more pronounced difference (and therefore a more pronounced anisotropy) between the magnetoresistances obtained for two orientations of the field which is due, most likely, to the highest alignment degree of the SWCNTs in the fabrication process. For both the structures, the perpendicular MR is negative with an upturn around $B = 3$ T.

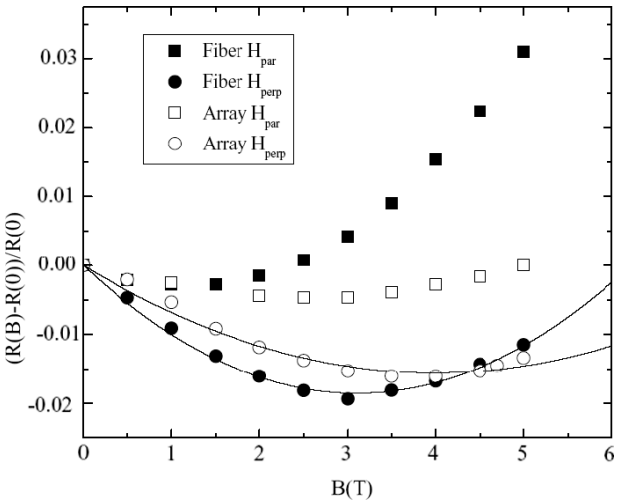

Figure 3. Magnetoresistance in both parallel and perpendicular (with respect to the fibre and bundle axes) magnetic field. The lines are fitted to the data according to equation (3).

Negative perpendicular MR is experimentally observed in disordered systems [17–23] where the VRH [17–20] or FIT [24] mechanisms work. Nevertheless, a systematic calculation of the dependence of MR on magnetic field and temperature has been developed in the framework of VRH theory [14, 20, 25] even though it is qualitatively accepted also in the case of FIT [24]. In the presence of an impurity (in VRH) or a potential barrier (in FIT), the decrease of the resistance at low or moderate magnetic field is due to the possible interference effects caused by the overlapping of the wavefunctions between two neighboured states. The effect is less pronounced for states far apart and for high and large barriers where the overlapping probability is reduced. Moreover, for a given distance or barrier the effect decreases at high magnetic field because of a shrinkage of the electron wavefunction which, in turn, reduces the overlapping between neighbouring states, giving a positive MR . Assuming that the two effects can be added [18, 20] if they work in different regimes, a phenomenological

expression for magnetoresistance is given by

$$\mathrm{MR} = -aB + bB^2 \tag{3}$$

where $a = c_{\mathrm{sat}}/H_{\mathrm{sat}}$ and $b \cong t_1(e^2a_0^4/\hbar^2)\,(T_{\mathrm{M}}/T)^{3/4}$. In these expressions, c_{sat} is a constant, $H_{\mathrm{sat}} = 3h/(ea_0^2)\,(T/T_{\mathrm{M}})^{3/8}$, $t_1 = 0.002\,48$, e is the electron charge and $a_0 \cong \xi$. Equation (3) is valid in the limit of low fields $B < B_{\mathrm{c}} = (6\hbar/ea_0^2)\,(T_{\mathrm{M}}/T)^{-1/4}$. Following the VRH theory, the a and b parameters are related to the different mechanisms that influence the electron wavefunction in the localization regime when a magnetic field is applied. In particular, the linear term takes into account the electron wavefunction interference whereas the quadratic term comes from the electron waveform shrinkage mechanism. As shown in figure 3, the MR is well fitted by equation (3) in the whole range of the data. The values of a and b obtained by the fit are reported in table 1. The value of the parameter a is lower in the case of the array than for the fibre, meaning that interference in the array is much less pronounced. A calculation of a_0 from the expression of the parameter b at $T = 4.2$ K gives an estimate of ξ for the two systems and, as a consequence, an estimate of the hopping length $r = (0.38)\,(T_M/T)^{1/4}\,\xi$. In fact, considering the T_{M} values obtained by the resistive data fitting with the 3D VRH model, one obtains the values of ξ reported in table 1. The substitution of these values inside the expression for B_c returns the value of 26 T as the upper limit of validity of equation (3), confirming that the condition $B \ll B_c$ is satisfied and the regime of applicability of equation (3) for our range of fields is confirmed.

The hopping lengths that we have obtained at $T = 4.2$ K for the arrays of bundles and for the fibres from the fittings based on equation (3) are reported in table 1. The values of the hopping length r give interesting indications on the dimensionality of the systems and on the transport mechanism inside the fibre and the bundles. The values of r are larger than the diameter of the inner SWCNT of the fibres or of the bundles of the arrays, but shorter than the bundles and fibre outer diameters. This condition suggests that the charge carriers inside each bundle/fibre move in a 3D environment finding very little resistance at the SWCNT–SWCNT junctions. Thus, we have a strong indication that the potential barrier of SWCNT–SWCNT interfaces inside fibres and bundles are weak and that the main part of the electrical resistance results from the intrinsic resistance of each SWCNT and from the action of the junctions between the outer interfaces.

5. Current–voltage characteristics

The current–voltage (I–V) characteristics traced for all the examined samples at negative and positive current showed no asymmetries nor rectification effects as shown in figure 4 for two typical samples (for the arrays the vertical scale is the one on the left while for the fibres it is the one on the right). This result suggests that Schottky mechanisms, if present, do not have a relevant role in our experiments. In order to estimate V_0 (the important parameter relative to equation (2)) we performed I–V measurements at different temperatures. All the curves, obtained by the four-probe technique, show a semiconducting behaviour at low temperature with an evolution towards ohmic linear shape at high temperature well above T^*. Representative curves are shown in figure 5(a) for the case of the fibre. A qualitative dependence of the barrier voltage V_γ can be extracted from these curves as a function of the temperature by a linear extrapolation to $I = 0$, as indicated in the figure for the rightmost I–V (the value of V_γ is indicated in the figure where the line intersects the horizontal axis). This dependence, after the normalization of V_γ with respect to the sample length, is reported in the inset of figure 5(a) for both samples. Considering V_γ as dependent on the energy of the barrier inside the sample, we can see that its value, as expected, increases on lowering the temperature and saturates at low temperature. In particular, the temperature at which this saturation is approached is consistent with T^* found by R versus T measurements (lower even now for the fibre with respect to the array). This result suggests that the presence of the potential barriers inside the systems starts to play a significant role at low temperature and affects the conductivity. Moreover, the much lower value of the potential (per unit length) obtained in the case of the fibre reflects the more compact structure of this system where the inner SWCNTs are tightly packed favouring the electrical conduction.

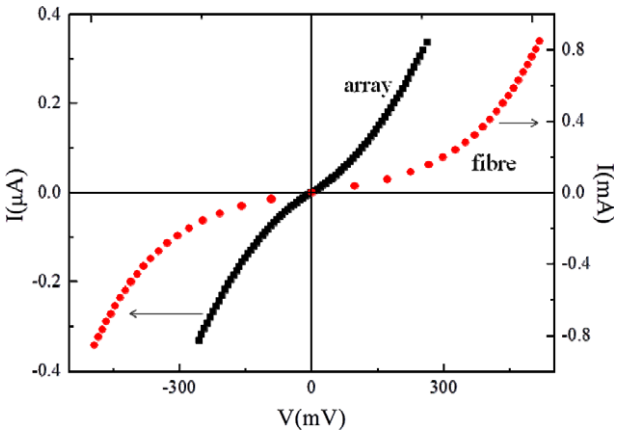

Figure 4. Typical I–V characteristic at $T = 4$ K for fibres and bundles. The symmetry of the curves with respect to current/voltage polarization indicates that Schottky-like barrier effects are negligible in the investigated ranges of voltage and currents.

In figures 5(b) and (c) the I–V curves for the two samples acquired at $T < T^*$ figure 5(b) and at $T > T^*$ figure 5(c) have been compared. The curves in figure 5(b) are fitted to the data following the equation obtained by the FIT model [26]:

$$I = \frac{G_0 V \mathrm{e}^{V/V_0}}{1 + h(\mathrm{e}^{V/V_0} - 1)} \tag{4}$$

where G_0 is the low current conductance at the same temperature of the I–V characteristic, $h = G_0/G_\gamma$, where $G_\gamma > G_0$ gives the ideal conductance in the case of no barriers and V_0 is the same barrier height present in equation (2). In the case of $h = 0$ equation (4) reduces to the diode characteristics. Moreover, by its definition, a negative h value would be

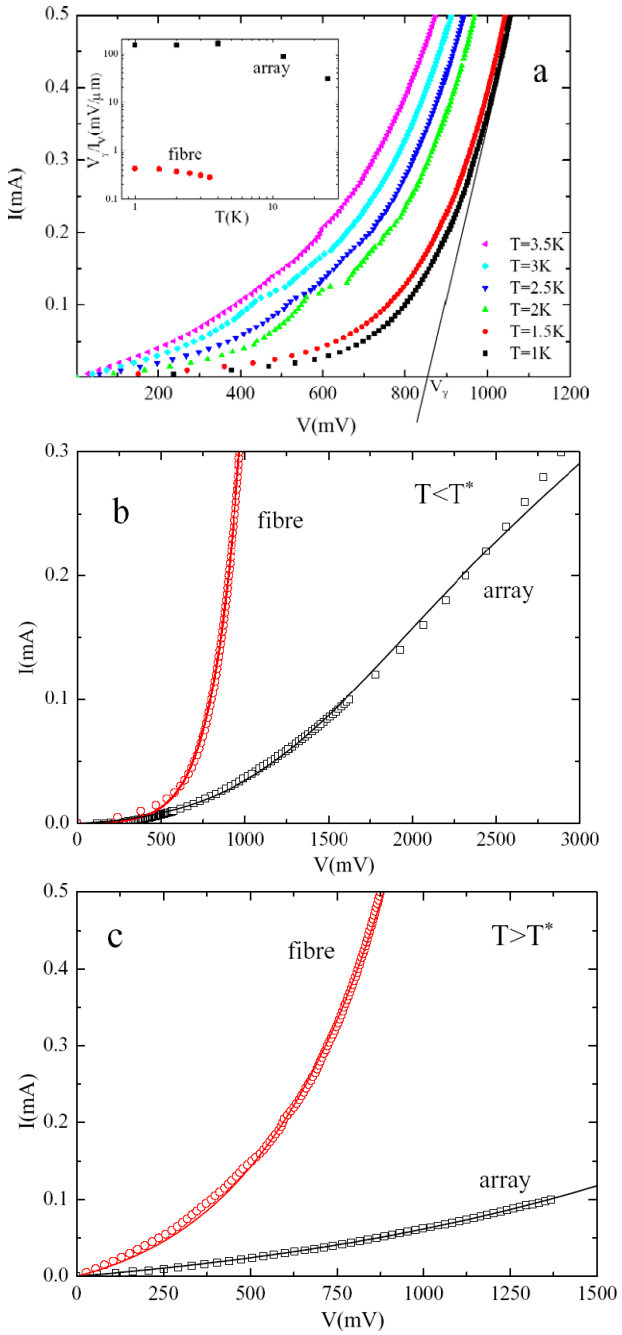

Figure 5. (a) *I–V* characteristics at different temperature for the fibre. The straight line shows the method adopted to determine the voltage gap V_γ for all the curves. Inset: temperature dependence of the voltage gap V_γ for both the fibre (circles) and the array (squares). (b) *I–V* for fibre (circles) and array (squares) at $T = 1$ K. (c) *I–V* for fibre (circles) and array (squares) at $T = 3.5$ K and $T = 12$ K, respectively. In (b) and (c) the lines fitting the data are the predictions of FIT equation (4) and VRH equation (5), respectively.

unrealistic. For $T < T^*$ all the *I–V* characteristics are well fitted by equation (4) while for $T > T^*$ unrealistic $h < 0$ values have been obtained, in agreement with the fact that the FIT model works at $T < T^*$ as indicated by R versus T measurements. The fits are obtained measuring G_0 by the R versus T method and using h and V_0 as fitting parameters. The values of V_0 obtained by the fitting procedure at $T = 1$ K are reported in table 1. In the case of the arrays, the value found is consistent with that observed by us and other authors for other samples in the low current bias limit. The substitution of these V_0 values inside the T_1/T_0 expression of the FIT model allows us to estimate the width w of the potential barrier. The results of calculation are reported in table 1. These values are realistic if compared to the van der Waals bonding length ($w > 1.34$ Å) and to the hopping distance as extracted from the R versus T data. The condition $r > w$ is, in fact, necessary if one assumes that interference or overlapping effects between wavefunctions related to neighbouring states are at the base of the considered theory.

The curves in figure 5(c) are fits to the data following the VRH model [21] and valid at moderate electric fields:

$$I = G_0 V e^{V/V_0}. \tag{5}$$

The agreement with the experimental data found here confirms that the aggregates behave as expected for a VRH regime when $T > T^*$.

6. Conclusions

The values of the physical constant obtained by the comparison between the models and the experimental data in the regimes of interest provide relevant information on the transport properties for aggregates of SWCNTs. At temperature higher than a given value T^*, the charge motion is well described by 3D VRH theory according to which the electron wavefunction is assumed to be localized on a distance ξ. Electron motion in this regime is characterized by hopping along a length r which is much longer than the width of the barrier generated by the junction between different SWCNTs or bundles and the heights of the barriers are too low to have some effect on the charge dynamics. When the temperature decreases, the barrier energy increases and this results in a freezing of the hopping effect. In this regime, which takes over when $T < T^*$, the conductance is not vanishing because of the tunnel effect (eventually enhanced by thermal fluctuation) and is strongly dependent on the barrier energy whose nature depends on the fabrication process of the aggregate. The stronger the connection is between two different bundles or SWCNTs, the weaker is the barrier energy and the lower is the temperature where the effect of this barrier becomes relevant.

In conclusion we can say that we have provided evidence that VRH and FIT theories are not competing models for the description of conduction phenomena in nanotube aggregates: indeed we have provided quantitative evidence that the two models can both describe the transport properties of aggregates of SWCNTs in different ranges of temperature.

Acknowledgment

The financial support of the Regione Lazio through the GESTO program is gratefully acknowledged.

References

[1] Kaiser A B 2001 *Rep. Prog. Phys.* **64** 1

Saito R, Dresselhaus G and Dresselhaus M S 1998 *Physical Properties of Carbon Nanotubes* (Singapore: World Scientific)
[2] Fuhrer M S *et al* 2000 *Science* **288** 494
[3] Bockrat M, Cobden D H, McEuen P L, Chopra N G, Zettl A, Thess A and Smalley R E 1997 *Science* **275** 1922
[4] de Heer W A, Bacsa W S, Chatelain A, Gerfin T, Baker R H, Forro L and Ugarte D 1995 *Science* **268** 845
[5] Terranova M L *et al* 2007 *J. Phys.: Condens. Matter* **19** 2255004
[6] Ericson L M *et al* 2004 *Science* **305** 1447
[7] Zhou W *et al* 2004 *J. Appl. Phys.* **95** 649
[8] Islam M F, Rojas E, Bergey D M, Johnson A T and Yodh A G 2003 *Nano Lett.* **3** 269
[9] Salvato M, Cirillo M, Lucci M, Orlanducci S, Ottaviani I, Terranova M L and Toschi F 2008 *Phys. Rev. Lett.* **101** 246804
[10] Fuhrer M S, Holmes W, Richards P L, Delaney P, Louie S G and Zettl A 1999 *Synth. Met.* **103** 2529
[11] Salvato M *et al* 2011 Macroscopic effects of tunnelling barriers in nanotube bundles aggregates arXiv:0904.2711
[12] Mott N F and Davis E A 1979 *Electronic Processes in Non-Crystalline Materials* (Oxford: Clarendon)
[13] Shklovskii B L and Efros A L 1984 *Electronic Properties of Doped Semiconductors* (Berlin: Springer)
[14] Sheng P 1980 *Phys. Rev.* B **21** 2180
[15] Badaire S, Pichot V, Zakri C, Poulin P, Launois P, Vavro J, Guthy C, Chen M and Fisher J E 2004 *J. Appl. Phys.* **96** 7509
Danilchenko B A, Shpinar L I, Tripachko N A, Voitsihovska E A, Zelensky S E and Sundqvist B 2010 *Appl. Phys. Lett.* **97** 72106
[16] Faran O and Ovadyahu Z 1988 *Phys. Rev.* B **38** 5457
[17] Vavro J, Kikkawa J M and Fischer J E 2005 *Phys. Rev.* B **71** 155410
[18] Jaiswal M, Wang W, Fernando K A S, Sun Y P and Menon R 2007 *Phys. Rev.* B **76** 113401
[19] Benzaquen M, Walsh D and Mazuruk K 1988 *Phys. Rev.* B **38** 10933
[20] Rosenbaum R 2001 *Phys. Rev* B **63** 94426
[21] Ksenevich V K *et al* 2008 *J. Appl. Phys.* **104** 73724
[22] Yosida Y and Oguro I 1999 *J. Appl. Phys.* **86** 999
[23] Rosenbaum R 2001 *Phys. Rev.* B **63** 94426
[24] Pakhomov A B, Zhang X X, Liu H, Wang X R, Huang H J and Yang S H 2000 *Physica* B **279** 41
[25] Kawabata A 1980 *Solid State Commun.* **34** 431
[26] Kaiser A B and Park Y W 2005 *Synth. Met.* **152** 181